Article

Functionalized Surfaces with Tailored Wettability Determine Influenza A Infectivity

Ilaria Mannelli, Ramon Reigada, Irina Suárez, Davide Janner, Albert Carrilero,
Prantik Mazumder, Francesc Sagués, Valerio Pruneri, and Melike Lakadamyali

Just Accepted

Functionalized Surfaces with Tailored Wettability Determine Influenza A Infectivity

Ilaria Mannelli,[*,†] Ramon Reigada,[‡,¶] Irina Suárez,[†] Davide Janner,[†] Albert Carrilero,[†] Prantik Mazumder,[§] Francesc Sagués,[‡,∥] Valerio Pruneri,[*,†,⊥,#] and Melike Lakadamyali[*,†,#]

†ICFO-Institut de Ciencies Fotoniques, The Barcelona Institute of Science and Technology, 08860 Castelldefels (Barcelona), Spain

‡Departament de Química Física, Universitat de Barcelona, Barcelona, Spain

¶Institut de Química Teòrica i Computacional (IQTCUB), Universitat de Barcelona, Barcelona, Spain

§Corning Incorporated, Sullivan Park, Corning, New York 14831, United States

∥Institut de Nanociéncia i Nanotecnologia (IN2UB), Universitat de Barcelona, Barcelona, Spain

⊥ICREA-Institució Catalana de Recerca i Estudis Avançats, Passeig Lluís Companys, 23, 08010 Barcelona, Spain

#These authors contributed equally to this work

E-mail: ilaria.mannelli@icfo.es; valerio.pruneri@icfo.es; melike.lakadamyali@icfo.es

Abstract

Surfaces contaminated with pathogenic microorganisms contribute to their transmission and spreading. The development of "active surfaces" that can reduce or eliminate this contamination necessitates a detailed understanding of the molecular mechanisms of interactions between the surfaces and the microorganisms. Few studies have

shown that, among the different surface characteristics, the wetting properties play an important role in reducing virus infectivity. Here, we systematically tailored the wetting characteristics of flat and nanostructured glass surfaces by functionalizing them with alkyl- and fluoro-silanes. We studied the effects of these functionalized surfaces on the infectivity of Influenza A viruses using a number of experimental and computational methods including real-time fluorescence microscopy and molecular dynamics simulations. Overall, we show that surfaces that are simultaneously hydrophobic and oleophilic are more efficient in deactivating enveloped viruses. Our results suggest that the deactivation mechanism likely involves disruption of the viral membrane upon its contact with the alkyl chains. Moreover, enhancing these specific wetting characteristics by surface nanostructuring led to an increased deactivation of viruses. These combined features make these substrates highly promising for applications in hospitals and similar infrastructures where antiviral surfaces can be crucial.

Keywords

Influenza A, wettability, hydrophobic and oleophilic surfaces, coarse-grained molecular dynamics simulations, fluorescence microscopy, nanostructured substrates

1   Introduction

Pathogenic microorganisms are abundant in the environment and their transmission may occur through several paths including contact with contaminated surfaces.[1] This route of transmission provides a big opportunity for the development of surfaces with special coatings, geometries or compositions that deactivate the microorganisms through contact and reduce their spreading.[2–8] The adsorption of microorganisms on surfaces involves several non-covalent intermolecular interactions such as ionic, hydrophobic, double layer, van der Waals, and hydrogen bonding.[9] Therefore, the interaction of surfaces with microorganisms

as well as their effects on the microorganism structure and activity can be tailored by tuning their physicochemical characteristics.[10] In the case of bacteria and enveloped viruses, their lipid membrane constitutes an excellent target for deactivation since it is readily accessible.

It has been shown that compounds with lipophilic moieties can interact with the membrane of bacteria and enveloped viruses, leading to their disruption.[5,11–13] In particular, studies using amphipathic compounds, such as antimicrobial peptides and graphene oxide sheets, have demonstrated their strong effect on the bacterial membrane. The former triggers lipopeptide-based responses on the bilayer structure, including changes in order and curvature, whereas the latter leads to lipid extraction that induces serious membrane stress and significantly reduces cell viability.[5,14–16] Similarly, branched hydrophobic polycations having long alkyl chains can be used as surface coatings to break the external membrane of enveloped viruses.[17] In all cases, the mechanism of disruption was ascribed to hydrophobic interactions. However, a systematic study that examines this mechanism as a function of other physicochemical properties of the surface in addition to hydrophobicity is lacking. Therefore, whether additional surface characteristics exist that also play a role in microorganism disruption is unclear. Studying the mechanism by which substrates with different wettability can interact with the lipid envelope of bacteria and viruses is thus timely and important since it can allow the design of new and more effective antimicrobial surfaces.

The wetting properties of surfaces can be tailored by functionalization with self-assembled monolayers (SAMs) of non-reactive molecules and also through micro/nano-structuring. Several treatments have been proposed for modifying the wetting properties of substrates in various applications, and to provide them with protective, self-cleaning, anti-fouling and anti-icing characteristics.[18–25] Here, we focused on hydrocarbon and fluorocarbon silanes since they are widely used for tuning the wettability of oxide materials and, moreover, they can serve as model systems and fundamental starting points for the development of new surfaces with antiviral properties.[17,26,27] We fine-tuned both the hydrophobic/hydrophilic and oleophobic/oleophilic character of glass substrates by depositing SAMs of hydrocarbon and

fluorocarbon silanes having different chain lengths, and studied how the wetting properties of these surfaces affect the integrity and infectivity of Influenza A viruses, a model system for enveloped virus.

We found that hydrophobicity alone is insufficient to describe the effect that a surface has on the integrity and infectivity of Influenza A viruses. Instead, hydrophobic and oleophilic interactions simultaneously play a major role in reducing viral infectivity. Molecular dynamics simulations of a variety of SAMs interacting with simple lipid vesicles provided additional insight into the molecular mechanism that led to lipid membrane disruption, and confirmed that highly hydrophobic and oleophilic coatings are the most effective in virus disruption. Real-time fluorescence microscopy observations further suggested that the viral particle splits apart upon contact with these surfaces, likely due to the disruption of the lipid envelope. Importantly, wetting properties were enhanced in nanostructured coatings with respect to their smooth counterparts, such that the use of nanostructured surfaces treated with hydrophobic/oleophilic SAMs demonstrated the strongest virus deactivation effect.

2 Experimental section

2.1 Surface functionalization

Substrates for self-assembled monolayers (SAMs) deposition were, firstly, cleaned by 5 min ultrasound treatments in acetone, ethanol, 3% solution of Deconex OP121 in milliQ H_2O, and milliQ H_2O. Successively the surfaces were activated by 30 min exposure to UV-O_3 cleaning treatment, 30 min dipping in a diluted base piranha solution (H_2O:H_2O_2:NH_3=5:5:1, used only with flat surfaces), and 10 min exposure to O_2 plasma. 1 mm thick glass slides were used for the infection activity measurements, while 0.1 mm thick glass slides were for the real-time imaging. SAMs of trichloro(methyl)silane, trichloro(propyl)silane, trichloro(hexyl)silane, trichloro(octyl)silane, trichloro(dodecyl)silane, trichloro(octadecyl)silane have been formed on the substrates by wet chemistry, using a 5 mM solution in toluene.[28] Trichloro-(3,3,4,4,5,5,

6,6,7,7,8,8,8-tridecafluorooctyl)-silane and trichloro-(3,3,4,4,5,5,6,6,7,7,8,8,9,9,10,10,11,11,12, 12,12-henicosafluorododecyl)-silane have been deposited by thermal evaporation. Both hydrocarbon and fluorocarbon silanes were from Sigma-Aldrich. In order to characterize the wetting properties of the substrates, the water and hexadecane contact angles were measured and averaged at three different positions on the surface of samples.

2.2 Viruses and Fluorescent Labelling

Influenza A virus X-31 was purchased from Charles River Laboratories (INFLUENZA X-31, A/AICHI/68). For these experiments, the purified product delivered as 2 mg/ml solution was used. Influenza A viruses are roughly spherical particles, ranging from 80 to 120 nm in diameter. The external membrane is composed by a lipid double layer characterized by the presence of approximately 500 spike-like projections, which are the envelope glycoproteins haemagglutinin (HA) and neuraminidase (NA).[29] To label with lipophilic dyes, the viruses were incubated with a 25 mM 1,1'-dioctadecyl-3,3,3',3'-tetramethylindodicarbocyanine (DiD, molecular Probes) solution in 50 mM HEPES buffer (pH 7.4, 145 mM NaCl) for 2 hours at 22°C. Unbound dye was removed via buffer exchange into the HEPES buffer using gel filtration columns NAP5 (GE Healthcare Life Sciences).

2.3 Real-time imaging of fluorescent labelled viruses

The behavior of viruses in contact with the functionalized surfaces was monitored in real time with a custom-built wide-field fluorescence microscope system based on an inverted Olympus IX71 microscope frame and equipped with a 100X 1.4 numerical aperture (NA) oil immersion objective. The slide was mounted on the microscope stage and 50-100 μl of X-31 virus solution (2 mg/ml) diluted $1:10^4$ with 50 mM HEPES buffer (pH 7.4) containing 145 mM NaCl, 2% Glucose and 1% solution of Glucose oxidase and Catalase, were deposited on the surface with a micropipette. In addition, in order to have a reference image of disrupted viral particles, a control test was performed by imaging the effect of a detergent

(1% sodiumdodecylsulfate (SDS) solution in water), able to disrupt the viral envelope, on viruses absorbed on bare glass surface. Live imaging was performed by using a laser light at 647 nm from a multichannel argon-krypton laser (Spectrum IC70, Coherent) for exciting DiD (excitation peak: 647 nm, emission peak: 669 nm). The emitted light was collected by the same objective and filtered by an emission filter (ET705/72m, Chroma) and imagined onto the EMCCD (Andor Technology) camera at a frame rate of 500 ms per frame.

Fiji, an open source image processing package, released under the General Public License,[30] was used for analysing the movies obtained from the fluorescence real-time imaging. The dimensions of large field of view images and videos were 40x40 μm^2, while zoomed pictures on single virus were 7.5x7.5 μm^2.

2.4 Cell culture

African green monkey kidney cells (BS-C-1, American Type Culture Collection, ATCC) were maintained in culture using a complete growth medium (Minimum Essential Medium Eagle with Earle's salts and nonessential amino acids plus 10% (vol/vol) FBS, 2 mM L-glutamine, and 1 mM sodium pyruvate; a penicillin streptomycin mixture was added to prevent bacterial contaminations) at 37°C and 5% CO_2. Cell culture media were purchased from GIBCO (Life Technologies). For the virus infectivity experiments, cells were plated on 8-well Lab-Tek 1 chambered coverglass (Nunc) at a seeding density of 20000-50000 cells per well.

2.5 Virus infectivity test

In all the experiments, the clean glass is used as reference substrate and the as prepared virus solution as positive control. The infection activity of the latter was evaluated at each set of experiments and the resulting percentage of infected cells was used as maximum value for the normalization of the data recorded during the experiment set. The infection activity of viruses after contact with the functionalized surfaces was evaluated using a two steps procedure. First a polystyrene media chambers was fixed on the functionalized surface

of the microscope slide using LOCTITE® Super Glue. Successively, 200 μl of X-31 virus solution (2 mg/ml) diluted 1:10^3 with modified Minimum Essential Medium (MEM), without L-Glutamine, HEPES and Phenol Red, from GIBCO (Life Technology) were added to the wells and left incubating 30 min. Afterwards, the virus solution was recovered and put in contact with the cell plated on the 8-well Lab-Tek 1 chambered coverglass (see section "Cell culture"). The growth medium was replaced with the virus solution and the infection process was left going on for 30 min at 37°C and 5% CO_2. Finally, the virus solution was removed from the cells and replaced with a modified MEM, with L-glutamine and Phenol Red, without HEPES, and containing 10 μg/mL trypsin. At this point the cells were left incubating for two days at 37°C and 5% CO_2. At the end of the incubating period, the infection extent is measured by means of the commercial kit D3® Double Duet™ DFA (Diagnostic Hybrids, Inc., USA), which contains viral antigen-specific murine monoclonal antibodies that are directly labelled with R-Phycoerythrin (excitation peaks = 490 nm and 565 nm, emission peak = 575 nm). Moreover, Fluoroshield histology mounting medium (Sigma-Aldrich), with 4,6-diamino-2-phenylindole (DAPI, excitation peak = 360 nm, emission peak = 460 nm), is used for labelling the cell nuclei.

The evaluation of the infection degree in cell cultures that were infected with virus solutions was done by calculating the ratio between the number of infected cells and the total of cells. Both numbers of cells were measured by imaging the cell culture with a Nikon inverted fluorescence microscope equipped with a 20X objective (NA=0.5). The total number of cells has been determined by illuminating the sample with the 405 nm laser that excites the DAPI molecules used for labelling the cell nuclei. On the other hand, the number of infected cells was obtained by illuminating the sample with the 561 nm laser in order to excite the R-Phycoerythrin molecules used as label tag in the commercial kit D3® Double Duet™ DFA. In each well, several images from different area of the surface were captured in order to have a statistically significant number of data for each sample.

Fiji software was used for the counting of (no)infected cells in the recorded images.

Successively, the ratios (number of infected cells)/(total number of cells), obtained for each substrate, were normalized to the positive control and compared in boxplot graphs.

In addition, in order to confirm the reliability of infectivity test results, two control experiments were performed. First, using fluorescence microscopy as described in section 2.3, we have quantified the amount of virus adsorbed onto the different surfaces during the period they are in contact with the virus solution by counting the number of fluorescent spots per field of view. The number of viruses on the surfaces was counted using the "Find maxima" tool available in Fiji software and adjusting the noise tolerance until all the visible spots were detected. Second, we have quantified the amount of virus contained in the solution that we could recover from the different surfaces by measuring the protein absorption peak using a NanoDrop UV-Vis spectrophotometer. Similarly to the infectivity test procedure, polystyrene media chambers were fixed on the surface using LOCTITE® Super Glue. Successively, 200 μl of X-31 virus solution (2 mg/ml) diluted 1:10 and 1:50 with 50 mM HEPES buffer (pH 7.4) containing 145 mM NaCl were added to the wells (three replicates for each sample) and left incubating 30 min. Afterwards, the virus solution was recovered and was treated with 0.1% SDS (sodium dodecylsulfate) solution by adding 20 μl of 1% SDS solution in H_2O to 180 μl of the recovered virus solution. The protein quantification was obtained by measuring the solution absorbance at 280 nm with a Nanodrop 2000c system (Thermo Fisher Scientific) and using a 70 μl UV-Cuvette micro (Brand). The conversion of absorbance to amount of protein was directly calculated by the instrument software using default parameters. The diluted stock solution that has not been in contact with the surface and treated with SDS was the positive control. Moreover, the blank for the absorbance measurements was made using the HEPES buffer employed for the dilution and containing 0.1% of SDS.

2.6   Molecular dynamics simulations

Simulations have been performed using the GROMACS v.4.5.5 software package[31] and the Martini v2.0 force field corresponding to a 4-to-1 coarse-grained description of the simulated

molecules[32] that has been successfully applied to study a variety of lipid membrane phenomena.[33] The coated surface consists of an impenetrable 25x25 nm^2 surface of 4900 fixed and regularly placed silica-like particles. In order to prevent water freezing in further steps, surface heterogeneity is accomplished by randomly replacing a 10% of the silica-like particles by similar but larger particles.[34] Coatings of 50x50 attached molecules have been simulated, which correspond to a lateral spacing of 0.5 nm, in accordance to experimental observations for alkylsilane monolayers.[35,36] Different moieties varying the length and polar characteristics are attached to the solid surface by fixing their first particle bead to the surface. Alkane molecules of 1, 2 and 3 apolar beads are simulated linked to fixed particles mimicking the silane group that links the molecule to the surface. These three moieties would correspond to silanes of butane, octane and dodecane, respectively. The polar coating has been built by replacing the non-fixed bead of the silane of butane by a polar bead. In order to mimic the effect of fluorinated silanes, alkane beads are replaced by particles with the same apolar character but 35% larger in radius according to what it is reported from detailed atomistic simulations.[37]

The simulated vesicles were built with 614 POPC and 263 Chol molecules (30 mol% of Chol), hydrated with 71552 water particles and conveniently equilibrated using a NpT ensemble (T=310 K, p=1 bar). A 15% of anti-freeze waters[32] was used in order to prevent anomalous water freezing. The vesicle equilibrium size is about 10 nm in diameter, 427 POPC molecules forming the outer leaflet and 187 POPC molecules in the inner leaflet. Chol molecules flip-flop frequently between the two leaflets, the inner layer being more concentrated in Chol (35-40 mol%). Both leaflets display a fluid behavior, and no holes/pores are observed. Water density inside and outside the vesicle becomes stabilized around 980 gr/l. Equilibrated vesicles are deposited on the top of the self-assembled monolayer and the production runs are then performed. The initial distance between the vesicle and the coated surface is so short (of the order of a few layers of water molecules) that the contact takes place almost instantly. Periodic boundary conditions are applied in the x and y directions,

temperature is fixed to 310 K and the size of the x,y simulation plane is kept constant. The surface particles and the first beads of the self-assembled moieties are fixed to their original positions during the simulation. Electrostatic interactions were handled using a shifted Coulombic potential energy form and charges were screened with a relative dielectric constant ϵ_r=15. The time step was set to 20 fs. Due to the "smoothing" inherent to the coarse-grained potentials, the effective time scale is larger than the actual simulation time. Here we used the standard conversion factor of 4,[31] which is the speed-up factor needed to obtain the correct diffusional dynamics of coarse-grained water particles compared with real water molecules. Simulations of 4 μs have been performed for each monolayer/vesicle system.

Water and oil wettability of the simulated surfaces have been analyzed by depositing a box of 8x8x8 nm^3 with 3800 water particles and a box with 950 hexadecane (HD) molecules, respectively. Short simulations of 160 ns are enough to observe how water and HD wet the monolayer. The same simulation protocols explained before have been used for the wetting simulations. By computing the averaged profiles of equilibrium droplets and following a similar procedure than in reference[38] , the contact angles have been measured for all simulated surfaces (Figure 2).

2.7   Surface nanostructuring

Glass nanostructured surfaces are fabricated by creating nanoscale metal masks on glass followed by reactive ion etching of the latter. Ultrathin metal films are first deposited on the flat glass surface. In a subsequent and rapid thermal annealing step the metal film is dewetted into discrete nanoparticles. These metal nanoparticles are subsequently used as masks during reactive ion etching of the surface. After removal of the metal masks, the surface is covered by monolithically integrated nanopillars whose geometry could be controlled by the process conditions. Details of the process could be found in reference[39] .

3   Results and discussion

3.1   Effects of hydrophobic surfaces on Influenza A infectivity

To determine the impact of substrate wetting on viral infectivity we developed a protocol to measure the level of infection after viruses have been in contact with the functionalized surface of interest (see Experimental section). Briefly, we recovered the virus solution from the surface after 30 mins of contact and infected BS-C-1 cells with the recovered viruses for 48 hours. We then determined the percentage of infected cells using a kit that contains a mixture of fluorescently labelled murine monoclonal antibodies directed against respiratory viral antigens, while DAPI was used to stain the nuclei of all cells (Figure 1a). Clean bare glass was used as reference and the infectivity levels were normalized to the value for the stock solution that did not come in contact with any surface (taken as 100% infection). For each substrate, the wetting properties were measured using the water contact angles (CAs) (see Table S1). In addition, the amount of virus adsorbed onto each surface was counted using fluorescence microscopy (see Experimental section) and found to be several orders of magnitude smaller than the total amount of viruses sampled in the infectivity test and comparable among different surfaces (68 ± 6 for bare glass, 47 ± 3 on (3,3,4,4,5,5,6,6,7,7,8,8,8-tridecafluorooctyl)silane and 40 ± 3 on (octadecyl)silane coated surface). The amount of virus recovered from bare glass and functionalized surfaces was further quantified using NanoDrop spectrophotometer and was similar among different surfaces and almost at the level of stock virus solution (Figure S1), indicating that there was very little virus lost due to adsorption. Thus, virus adsorption to the surface likely does not play a significant role in the changes observed in infectivity.

Figure 1b shows the relationship between the infectivity for viruses that have been in contact with glass surfaces modified with alkyl silanes $R\text{--}Si(OH)_3$, R varying from $-CH_3$ to $-(CH_2)_{17}CH_3$, and the water contact angles measured on these substrates (see Experimental section and Table S1). As it is evident from Figure 1b, hydrophilic surfaces did not
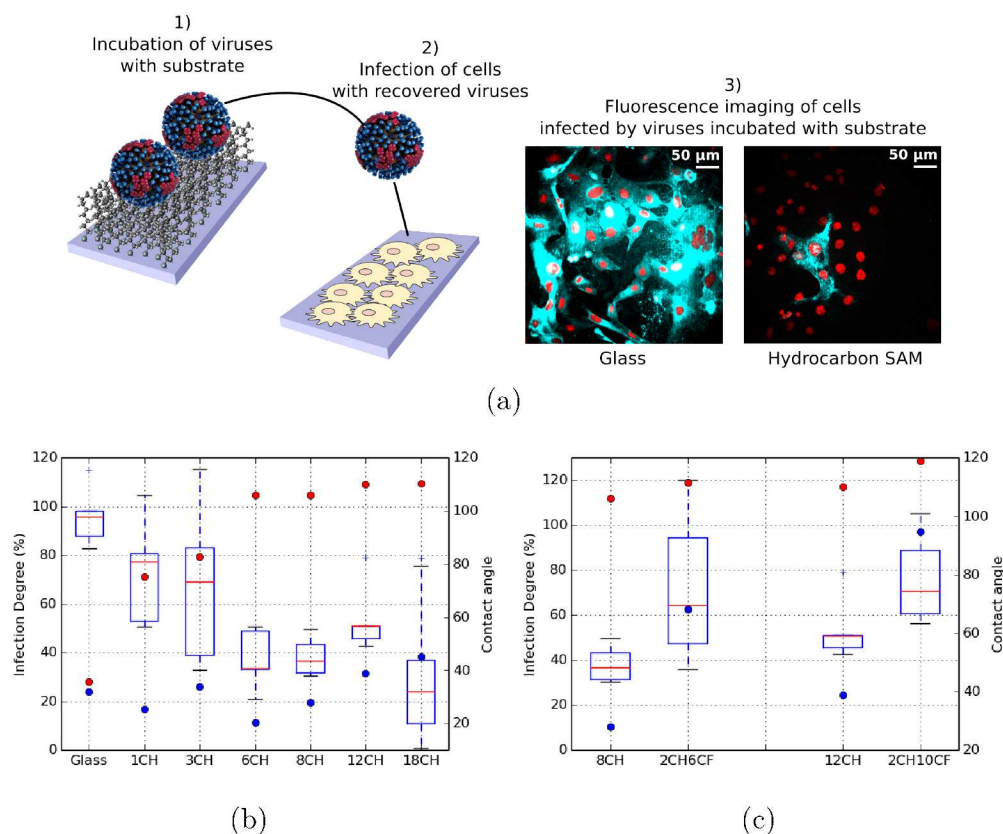
(a)

(b)

(c)

Figure 1: Effects of hydrophobic surfaces on viral infectivity. (a) Scheme of the virus infectivity test. Left: cartoon representation of viruses in contact with the functionalized flat or nanostructured surface and transfer of the viruses to the cell culture. Right: Imaging of the infectivity level on cells treated with viruses previously incubated with standard glass (left image) and a surface functionalized with a hydrocarbon silane SAM (right image). The red signal, from DAPI fluorescence, shows the nuclei of all cells in the culture, while the light blue signal, from the R-Phycoerythrin, does the infected cells. (b) Boxplots of the percentage infection level measured for hydrocarbon silanes having different alkyl chain lengths and their corresponding water (red dots) and hexadecane (blue dots) contact angles. (c) Boxplots of the percentage infection level measured for hydrocarbon and fluorocarbon silanes having the same chain lengths and their corresponding water (red dots) and haxadecane (blue dots) contact angles. The boxplot were plotted with n=5 for all samples except n=10 for the 18CH sample. The box bounds the interquartile range (IQR=Q3-Q1, where Q1 = first quartile (25th percentile) and Q3 = third quartile (75th percentile)) divided by the median (Q2, red horizontal bar), and Tukey-style whiskers extend to 1.5xIQR beyond the box. Q1-1.5xIQR > values > Q3+1.5xIQR are outliers (blue + symbols).

have significant effect on the infection level of Influenza A viruses. For example, the bare glass displayed a water CA equal to 36° and the resulting infection degree after contact was close to 100% (see Glass in Figure 1b). Similar results were obtained with SAMs of silanes having short alkyl chains $-CH_3$ and $-(CH_2)_2CH_3$ (labelled 1CH and 3CH in figure caption),

which changed water wettability only moderately towards more hydrophobic. In these conditions, the infection level was only slightly decreased compared to bare glass (Figure 1b). A significant decrease in the infection level was observed when using SAMs of longer alkyl chain: $-(CH_2)_5CH_3$, $-(CH_2)_7CH_3$, $-(CH_2)_{11}CH_3$ and $-(CH_2)_{17}CH_3$ (6CH, 8CH, 12CH, 18CH) for which the water CA increased significantly (Table S1). Overall, these results indicate that the infection degree drops when the water CA is 100° or greater, characteristic of a hydrophobic surface. As a further test, we substituted the alkyl- for fluoro-silanes, $-(CH_2)_2(CF_2)_5CF_3$ and $-(CH_2)_2(CF_2)_9CF_3$ (2CH6CF and 2CH10CF), which as expected increased the CA with water. Surprisingly, despite the dramatic increase in hydrophobicity, the infectivity decrease was lower than that observed with hydrocarbon functionalized surfaces (Figure 1c). This result suggests that the hydrophobic characteristics of a surface do play an important, although not unique, role in deactivating Influenza A viruses.

3.2 Molecular dynamics simulations of functionalized surface effects on viral envelope membrane

We realized that while the substitution of the alkyl- for fluoro-silanes increased surface hydrophobicity, it also rendered the surface more oleophobic as determined by measuring hexadecane contact angle (Figure 1b and 1c; Table S1). To gain deeper insight into how the combined hydrophobicity and oleophobicity may impact the molecular interactions between the surfaces and the viruses and lead to virus inactivation, we performed molecular dynamics (MD) simulations using a 4-to-1 coarse-grained (CG) description of the simulated molecules (see Experimental section). To capture the salient features of the interaction between the coated surfaces and Influenza A viruses, we modeled the virus as a small lipid vesicle representing its envelope. In addition, we replicated the substrate as a fused silica (SiO_2) surface on which silane molecules with different moieties varying in length and polar characteristics were attached by linking their silanol containing bead (Figure 2, black bead in CG molecules) to the silica particles of the surface. Three hydrocarbon silanes $R=(CH_2)_xCH_3$ (x=3, 7 and

11), and their fluorinated counterparts (fluorocarbons) were simulated, as well as a polar coating obtained by replacing the apolar bead of the shortest hydrocarbon moiety by a polar particle bead (Figure 2). Although the simulations are performed in the typical spatiotemporal scales used in Martini-based simulations,[33] it is important to note that the simulated vesicles are much smaller than real Influenza viruses. However, they can be considered as extremely simplified models for real viruses that serve as a benchmark systems to test the adhesion/destruction effect of the different tested monolayer coated surfaces. For this purpose, some vesicle membrane properties like in-plane fluidity and mechanical stiffness are likely more important than the vesicle size. In this respect, we used 30 mol% of cholesterol in the simulated vesicles to provide them with highly fluid and flexible membranes similar to those found for influenza virosomes.[40,41] Finally, the wetting characteristics (hydrophobicity and oleophobicity) of the monolayers were determined by simulating the behaviour of small drops of water (polar) and hexadecane (organic non-polar, oil) deposited on top of each of them (see Experimental section and Figure 2).

MD simulations revealed three distinct modes of action clearly explained by the combination of water and oil wettability (Figure 2). The first mode, in which the vesicle was not affected by the surface (Figure 2, Mode 1), was observed on hydrophilic/oleophobic polar silane coatings, having a very small water CA $<10°$ and a large hexadecane CA $>50°$. In this situation, no vesicle adhesion was observed since there was no energy gain by replacing the surface contact with water by the contact with the hydrophobic parts of the lipid vesicle molecules (Movie S1). In the case of the hydrocarbon monolayers corresponding to hydrophobic/oleophilic surfaces, we found a rather different mode of action (Figure 2, Mode 2). Shortly after the contact with the surface, the vesicle broke and a thimble-like intermediate structure was formed, which progressively spread over the surface forming a lipid monolayer of vertically-placed lipids on the top of the SAM (Movie S2). In this case, the interactions between the surface and water molecules were replaced by more favourable contacts with the hydrophobic parts of the lipid vesicle components leading to complete membrane dis-
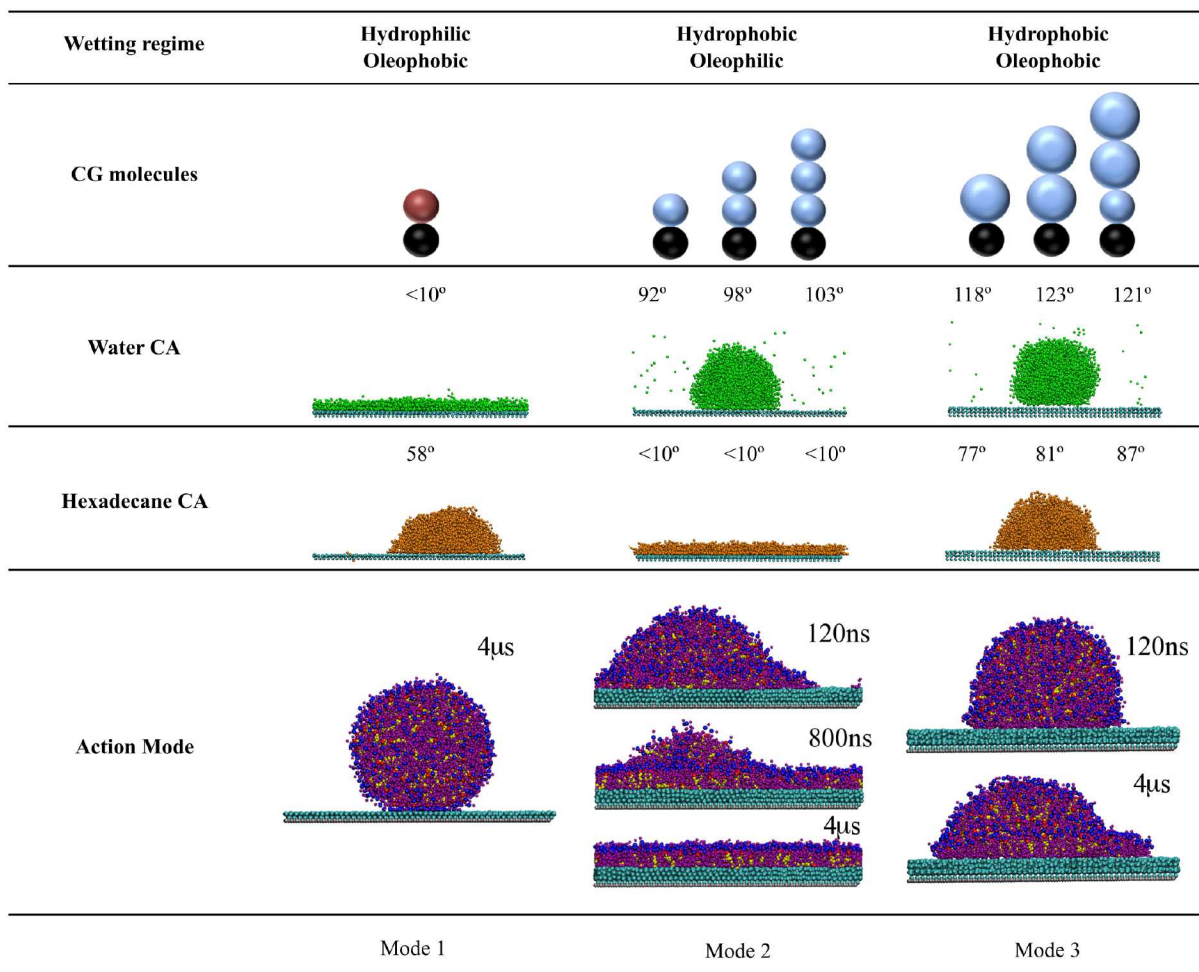
Wetting regime	Hydrophilic Oleophobic	Hydrophobic Oleophilic			Hydrophobic Oleophobic		
CG molecules							
Water CA	<10°	92°	98°	103°	118°	123°	121°
Hexadecane CA	58°	<10°	<10°	<10°	77°	81°	87°
Action Mode	4μs	120ns 800ns 4μs			120ns 4μs		
	Mode 1	Mode 2			Mode 3		

Figure 2: Summary of simulation results. (Upper panels) Wetting characteristics and schematic representation for the molecules forming the simulated monolayers. Black beads correspond to the silanol groups attached to the surface. Blue beads represent the apolar beads corresponding to four methylenes (normal size) or four fluorinated methylenes (large size). The red bead stands for a polar particle. (Middle panels) Contact angles and deposited droplets for water (up, in green) and oil (down, in orange). (Bottom panels) Final configuration of the vesicle in contact with polar (left), alkane (center) and fluorinated (right) coated surfaces. Colour code: POPC (magenta), cholesterol (yellow), PC headgroup (blue), cholesterol hydroxyl (red), assembled moieties (cyan) and silica surface (silver). Water molecules are not plotted for clarity. The complete sequence for the three cases is shown in supporting movies: Movie S1, Movie S2 and Movie S3.

ruption. Finally, for the fluorocarbon coatings, the vesicle initially came in contact with the surface and was partially adsorbed by the monolayer forming a rather stable thimble-like structure where the bilayer configuration was only preserved in the part of the vesicle not in contact with the surface (Figure 2, Mode 3, and Movie S3). In this latter case, fluorocarbon

SAMs showed highly hydrophobic behaviour but also a significant oleophobic character. In this situation, the interaction between the coating moieties and the hydrophobic tails of the membrane lipids was also penalized, so that an intermediate disruption effect was observed. A detailed analysis of the adhesion energy for the three reported cases can be found in Figure S2.

Overall, the simulations are in direct agreement with the experimental results and provide a molecular level explanation as to why the optimal condition for virus deactivation corresponds to surfaces that display simultaneously hydrophobic and oleophilic characteristics.

3.3   Real time imaging of influenza A virus interaction with functionalized surfaces

MD simulations demonstrated that the virus deactivation is caused by viral membrane disruption upon contact with the alkyl chains forming the SAM. To observe this process in real time, we labeled the lipid membrane of influenza A viruses using a lipophilic dye (DiD, see Experimental section) and imaged the interaction of individual viruses with the different surfaces using total internal reflection fluorescence (TIRF) microscopy.

Figure 3 shows frames from a real time video of viruses interacting with bare glass and 18CH coated glass surfaces, respectively (Movies S4a-b and S6a-b). In both cases, individual viruses can be observed to adsorb onto the surface and appear as diffraction limited spots soon after adding the viral solution. In the case of glass, these viruses remained as single diffraction limited spots throughout the whole observation period or until they unbound from the surface and disappeared (Figure 3a-3d and Movies S4a-b). Similar behavior was observed on hydrophilic and hydrophobic/oleophobic surfaces, which had little or no effect on the infectivity of the viruses (Movies S5a-b).

Interestingly, in the case of hydrophobic/oleophilic surfaces, the initial bright fluorescent viral particle started splitting into smaller pieces soon after the contact and the signal no
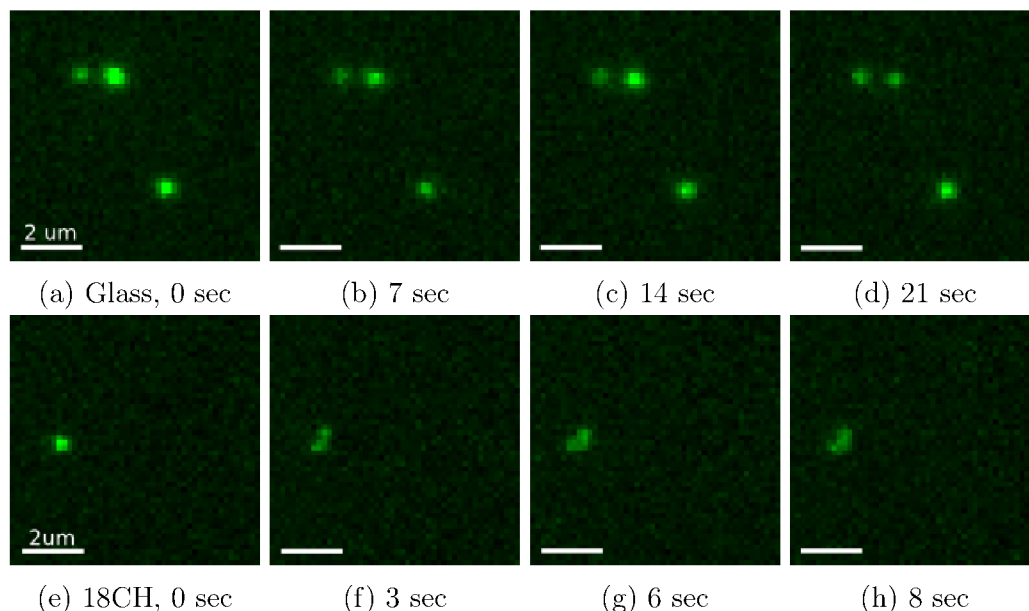
Figure 3: Real-time imaging of single Influenza A viruses on surfaces. Image dimensions: 7.5×7.5 μm^2. Images of single viruses recorded at different times on glass surface (a-d) and on 18CH coated surface (e-h).

longer resembled a diffraction limited spot (3 seconds, Figure 3e-3h, Movies S6a-b and S7). A similar behavior was observed on viruses absorbed on bare glass and treated with a detergent, which is able to disrupt the lipid bilayer of the virus envelope. Instead of remaining a well-defined diffraction limited spot, the images of viruses on hydrophobic/oleophilic surfaces as well as detergent-treated viruses showed several overlapping spots clustered in close proximity and spread over many pixels due to the splitting of the fluorescence signal into several pieces (Figure S3). As expected, the intensity profile of viruses on hydrophobic/oleophilic surfaces showed both a decrease in amplitude and broadening in width over time as the initial single virus spot split into pieces (Figure S4). In contrast, no broadening in the width of the intensity profile of viruses on glass was observed over time (Figure S4). The amplitude of the intensity profile for these viruses either remained constant or showed some modulation over time as the fluorescence signal either photobleached or moved in and out of focus (Figure S4). At long times (8 minutes) the fluorescence signal on functionalized active surfaces further spread into a uniform, large blob likely due to the leakage of the fluorescent dye from the disrupted lipid membrane (Figure S5). Since the fluorescent dye was incorporated inside the

17

viral membrane, the real time imaging suggests that the lipid bilayer was disrupted upon interaction of the viruses with hydrophobic/oleophilic surfaces. Indeed, previous live-cell single virus tracking studies using the same labeling strategy showed that this fluorophore can leak out of the viral membrane and spread into a larger area in living cells only after the fusion of the viral membrane with the membrane of acidic endosomes.[42,43] Prior to this fusion event, the fluorescence signal remains confined to a diffraction limited spot as we observe on bare glass. Once fusion of the two membranes takes place, the fluorescence spreads into a larger area of the endosome.[42,43]

3.4 Design and development of highly hydrophobic/oleophilic surfaces through nanostructuring

Based on the above results, we aimed to develop new functionalized surfaces that could enhance simultaneously hydrophobicity and oleophilicity. To this end, we took advantage of surface nanostructuring that can be easily achieved using metal dewetting techniques[39] (Figure 4a). When the nanostructured surface was coated with the $-(CH_2)_2(CF_2)_5CF_3$ (2CH6CF), both water and hexadecane contact angles increased compared to the flat glass with the same coating. Although hydrophobicity was enhanced, the simultaneous increase in oleophobicity led to a similar virus deactivation capability compared to the flat counterpart (Figure 4b).

On the other hand, when the nanostructured surface was coated with $-(CH_2)_{11}CH_3$ (12CH), the nanostructures rendered the surface superhydrophobic (water CA from 110° to 154°) as well as more oleophilic (hexadecane CA from 39° to 26°) compared to the flat glass coated with the same molecule. This surface led to a dramatic reduction in the infectivity level of viruses to below 10% (Figure 4b), the strongest deactivation capacity observed among all the surfaces tested. We hypothesize that this phenomenon is likely due to the relative differences of wetting regimes of the two phases - water and virus - on the nanostructured surface. With fluorocarbon coating over nanostructured surface, both hydrophobicity and
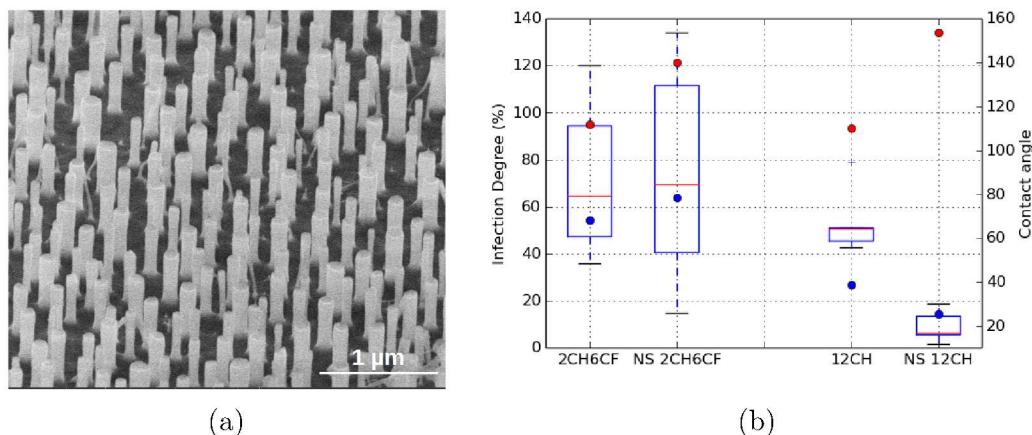
Figure 4: Effects of surface nanostructuring on viral infectivity. (a) SEM images of a nanostructured surface. Nanopillar height is ∼430 nm and the average diameter is ∼100 nm. (b) Boxplots of the percentage infection level measured for flat and nanostructured (NS) surfaces and their corresponding water (red dots) and hexadecane (blue dots) contact angles. The comparison was made for 2CH6CF and 12CH coated surface. The boxplot were plotted with n=5 for 8CH and 12CH samples, n=6 for the NS 12CH sample and n=10 for the NS 2CH6CF sample. The box bounds the interquartile range (IQR=Q3-Q1, where Q1 = first quartile (25th percentile) and Q3 = third quartile (75th percentile)) divided by the median (Q2, red horizontal bar), and Tukey-style whiskers extend to 1.5xIQR beyond the box. Q1-1.5xIQR > values > Q3+1.5xIQR are outliers (blue + symbols).

oleophobicity are amplified leading to Cassie-Baxter wetting regime for both phases. This in turn reduces the interaction (or interaction area) between the surface and the virus. On the other hand, with hydrocarbon coating, the hydrophobicity and oleophilicity are amplified leading to Cassie-Baxter and Wenzel wetting regimes for water and virus, respectively. This in turn has the effect of increasing the contact area between the virus and the nanostructured surface compared to that on the flat surface. It would be interesting in the future to investigate these proposed mechanisms in a systematic and quantitative way.

The results on nanostructured surfaces further support the hypothesis that the virus inactivation is due to the high affinity of the lipophilic moieties on the surface for the alkyl chain of the phospholipids that form the virus envelope. At the same time they suggest a new way to modify surfaces to be antiviral for important applications such as maintaining acceptable levels of hygiene in hospitals and public infrastructures and helping to fight the spread of hospital-acquired infections via the contamination of inanimate surfaces in the

healthcare environment.[44]

4   Conclusions

Surface contaminated with pathogenic microorganisms are known to contribute to their transmission and spreading, especially in sensitive environments like health care infrastructures. As reported in literature, the Influenza A viruses can remain active up to nine hours[45] and even days in case of pandemic types.[46] As a consequence, new surfaces or coatings that could reduce or completely eliminate microorganism adsorption and/or transmission are demanded for these specific real world applications; and, in this context, it is important to know and understand the nature of the interactions between microorganisms and surfaces. Our results provide important insights into the nature of the interaction between Influenza A viruses, a model system for enveloped viruses, and glass surfaces functionalized with self-assembled monolayer of chemically non-reactive compounds. Combining several approaches, including the simulation of the adhesion and disrupting actions of the different coatings, the experimental measurements of the infection level of viruses after their contact with the different substrates, and the real-time fluorescence imaging of viruses on each surface, we were able to elucidate the molecular mechanisms involved in the interaction of viruses with surfaces having tailored wetting properties. The experimental and simulation results were in excellent agreement and allowed us to suggest the design of new and more effective coating strategies.

Our results demonstrated that the combination of hydrophobic and oleophilic features is key for disrupting the lipid bilayer of the Influenza A virus and for rendering it unable to infect mammalian cells. The use of alkyl-silane coatings revealed the importance of hydrophobicity on the capacity of a surface to deactivate viruses: in the simulations, longer alkyl moieties resulted in more hydrophobic substrates and a stronger damaging action leading to complete vesicle destruction. This mechanism was in accordance with the real-time

imaging results showing, for long alkane monolayers, the spreading of the fluorescence signal associated to the viral envelope upon contact with the surface (Figure 3). Interestingly, the same destruction mechanism was proposed for the inactivation of Influenza A virus by hydrophobic polycations having twelve carbon alkyl chains as hydrophobic moieties.[17] Moreover, fluorescence microscopy studies on giant unilamellar vesicle adhesion and fusion to interfaces led to the development of a model in which the hemifusion process drives the vesicle disruption and the formation of a dense monolayer of lipids on the surface.[47]

Increasing hydrophobicity by the use of equivalent fluorocarbon silanes, however, did not increase its destructive effect. A similar effect was observed in a slightly different context for fluorinated antimicrobial peptides, which have reduced antimicrobial activity when they are highly fluorinated.[48] At this point, MD simulations revealed that fluorinated coatings displayed a significant energy penalty for the contacts between the tips of the molecules forming the monolayer and the hydrophobic lipid tails that impeded membrane disruption. For this reason, the oleophilic/oleophobic character of the surface coating has to be simultaneously considered. Simulation and experimental measurements of the water and hexadecane contact angles on the different surfaces showed that the higher destructive mode and lower infection degree were observed on hydrophobic and oleophilic substrates. This suggests that the low affinity of water for hydrophobic surfaces and the high attraction of phospholipid tails towards oleophilic surfaces are the driving forces that trigger virus envelope disruption.[49] Importantly, we experimentally demonstrated that boosting these wetting characteristics by nanostructuring the surfaces maximized their destructive effect on Influenza A virus.

Overall, our results give new insights into the role of the wetting properties of functionalized surfaces on their effect on enveloped viruses that come in contact with them. Moreover, and due to the bilayer nature of the viral envelope, this strategy might likely be extended to bacterial microorganisms also enclosed by lipid membranes, and will be subject to further studies. These results constitute the basis for guiding the design and development of new surfaces with higher antiviral activity that can be important for applications in public

and/or sensitive environments such as in hospitals.

Associated Content

Supporting Information Supporting figures, movies and table. This material is available free of charge via the Internet at http://pubs.acs.org.

Acknowledgement

References

(1) Weinstein, R. A.; Bridges, C. B.; Kuehnert, M. J.; Hall, C. B. Transmission of Influenza: Implications for Control in Health Care Settings. *Clin. Infect. Dis.* **2003**, *37*, 1094–1101.

(2) Carmona-Ribeiro, A. M.; de Melo Carrasco, L. D. Cationic Antimicrobial Polymers and Their Assemblies. *Int. J. Mol. Sci.* **2013**, *14*, 9906–9946.

(3) Plueddemann, E. P.; Revis, A. Organosilicon Quaternary Ammonium Antimicrobial Compounds. 1989; CIB: A01N55/00; A61K8/00; A61K8/55; A61K8/58; C07F7/18; (IPC1-7): C07F7/10.

(4) Monticello, R. A.; White, W. C. *Applied Biomedical Microbiology*; CRC Press, 2009; pp 45–58.

(5) Salwiczek, M.; Qu, Y.; Gardiner, J.; Strugnell, R. A.; Lithgow, T.; McLean, K. M.; Thissen, H. Emerging Rules for Effective Antimicrobial Coatings. *Trends Biotechnol.* **2014**, *32*, 82–90.

(6) Borrelli, N. F.; Morse, D. L.; Senaratne, W.; Verrier, F.; Wei, Y. Coated, Antimicrobial, Chemically Strengthened Glass and Method of Making. 2012; CIB: B32B17/10; B32B7/02; C03C17/30; C03C21/00; C03C3/00; C03C3/04; C03C3/083; C03C3/085; C03C3/087; C03C3/091; C03C3/093; C03C3/095.

(7) Borrelli, N. F.; Petzold, O. N.; Schroeder, J. F.; Senaratne, W.; Verrier, F.; Wei, Y.; Schroeder, I. J. F. Antimicrobial Action of Cu, CuO and Cu2O Nanoparticles on Glass Surfaces and Durable Coatings. 2015; CIB: A01N59/20; C03C17/00; C03C17/36; C03C17/42; C03C21/00; C03C3/04.

(8) Pilloy, G.; Hecq, A.; Hevesi, K.; Jacobs, N. Substrate with Antimicrobial Properties. 2006; CIB: C03C17/00; C03C17/34; C23C14/06; C23C14/34.

(9) Gerba, C. P. In *Advances in Applied Microbiology*; Laskin, A. I., Ed.; Academic Press, 1984; Vol. 30; pp 133–168.

(10) Dou, X.-Q.; Zhang, D.; Feng, C.; Jiang, L. Bioinspired Hierarchical Surface Structures with Tunable Wettability for Regulating Bacteria Adhesion. *ACS Nano* **2015**, *9*, 10664–10672.

(11) Teixeira, V.; Feio, M. J.; Bastos, M. Role of Lipids in the Interaction of Antimicrobial Peptides with Membranes. *Prog. Lipid Res.* **2012**, *51*, 149–177.

(12) Gerrard, S. E.; Larson, A. M.; Klibanov, A. M.; Slater, N. K.; Hanson, C. V.; Abrams, B. F.; Morris, M. K. Reducing Infectivity of HIV upon Exposure to Sur-

faces Coated with N,N-dodecyl, methyl-polyethylenimine. *Biotechnol. Bioeng.* **2013**, *110*, 2058–2062.

(13) Schmidtchen, A.; Pasupuleti, M.; Malmsten, M. Effect of Hydrophobic Modifications in Antimicrobial Peptides. *Adv. Colloid Interface Sci.* **2014**, *205*, 265–274.

(14) Horn, J. N.; Romo, T. D.; Grossfield, A. Simulating the Mechanism of Antimicrobial Lipopeptides with All-Atom Molecular Dynamics. *Biochemistry* **2013**, *52*, 5604–5610.

(15) Zasloff, M. Antimicrobial Peptides of Multicellular Organisms. *Nature* **2002**, *415*, 389–395.

(16) Tu, Y.; Lv, M.; Xiu, P.; Huynh, T.; Zhang, M.; Castelli, M.; Liu, Z.; Huang, Q.; Fan, C.; Fang, H.; Zhou, R. Destructive Extraction of Phospholipids from Escherichia coli Membranes by Graphene Nanosheets. *Nat. Nanotechnol.* **2013**, *8*, 594–601.

(17) Hsu, B. B.; Wong, S. Y.; Hammond, P. T.; Chen, J.; Klibanov, A. M. Mechanism of Inactivation of Influenza Viruses by Immobilized Hydrophobic Polycations. *Proc. Natl. Acad. Sci. U. S. A.* **2011**, *108*, 61–66.

(18) Kruszewski, K. M.; Gawalt, E. S. Perfluorocarbon Thin Films and Polymer Brushes on Stainless Steel 316 L for the Control of Interfacial Properties. *Langmuir* **2011**, *27*, 8120–8125.

(19) Kumar, V.; Pulpytel, J.; Rauscher, H.; Mannelli, I.; Rossi, F.; Arefi-Khonsari, F. Fluorocarbon Coatings Via Plasma Enhanced Chemical Vapor Deposition of 1H,1H,2H,2H-perfluorodecyl Acrylate - 2, Morphology, Wettability and Antifouling Characterization. *Plasma Processes Polym.* **2010**, *7*, 926–938.

(20) Miyagawa, H.; Yamauchi, K.; Kim, Y.-K.; Ogawa, K.; Yamaguchi, K.; Suzaki, Y. Fabrication of Transparent Antifouling Thin Films with Fractal Structure by Atmospheric Pressure Cold Plasma Deposition. *Langmuir* **2012**, *28*, 17761–17765.
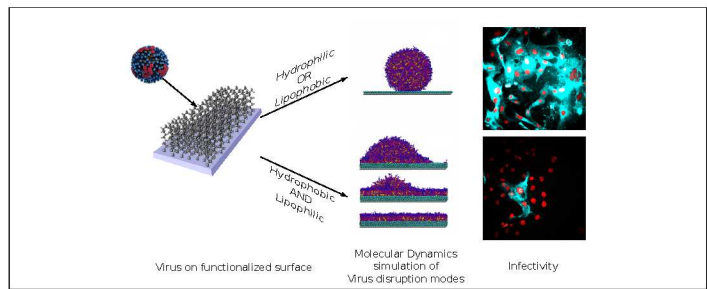
(21) Zhang, Y.; Qi, Y.-h.; Zhang, Z.-p.; Sun, G.-y. Synthesis of Fluorinated Acrylate Polymer and Preparation and Properties of Antifouling Coating. *J. Coat. Technol. Res.* **2014**, *12*, 215–223.

(22) Lee, S. B.; Park, i. J.; Ha, J. W.; Lee, K. W.; Lee, S. G.; Park, E. Y.; Kim, E. K. Per-Fluoro Polyether Compound, Antifouling Coating Composition and Film Containing Same. 2012; CIB: G11B5/64; C09J7/02.

(23) Lv, J.; Song, Y.; Jiang, L.; Wang, J. Bio-Inspired Strategies for Anti-Icing. *ACS Nano* **2014**, *8*, 3152–3169.

(24) Wittchow, E. Biocorrodible Implant with Anti-Corrosion Coating. 2014; CIB: A61F2/82; A61L31/10; A61L31/14.

(25) Yao, L.; He, J. Recent Progress in Antireflection and Self-Cleaning Technology âĂŞ From Surface Engineering to Functional Surfaces. *Prog. Mater. Sci.* **2014**, *61*, 94–143.

(26) Botequim, D.; Maia, J.; Lino, M. M. F.; Lopes, L. M. F.; Simões, P. N.; Ilharco, L. M.; Ferreira, L. Nanoparticles and Surfaces Presenting Antifungal, Antibacterial and Antiviral Properties. *Langmuir* **2012**, *28*, 7646–7656.

(27) Haldar, J.; Weight, A. K.; Klibanov, A. M. Preparation, Application and Testing of Permanent Antibacterial and Antiviral Coatings. *Nat. Protoc.* **2007**, *2*, 2412–2417.

(28) Ulman, A. Formation and Structure of Self-Assembled Monolayers. *Chem. Rev.* **1996**, *96*, 1533–1554.

(29) Drexler, M. *What You Need to Know About Infectious Disease*; National Academies Press (US): Washington (DC), 2010.

(30) Schindelin, J.; Arganda-Carreras, I.; Frise, E.; Kaynig, V.; Longair, M.; Pietzsch, T.; Preibisch, S.; Rueden, C.; Saalfeld, S.; Schmid, B.; Tinevez, J.-Y.; White, D. J.; Harten-

stein, V.; Eliceiri, K.; Tomancak, P.; Cardona, A. Fiji: an Open-Source Platform for Biological-Image Analysis. *Nat. Methods* **2012**, *9*, 676–682.

(31) Lindahl, E.; Hess, B.; Spoel, D. v. d. GROMACS 3.0: a Package for Molecular Simulation and Trajectory Analysis. *J. Mol. Model.* **2001**, *7*, 306–317.

(32) Marrink, S. J.; Risselada, H. J.; Yefimov, S.; Tieleman, D. P.; de Vries, A. H. The MARTINI Force Field: Coarse Grained Model for Biomolecular Simulations. *J. Phys. Chem. B* **2007**, *111*, 7812–7824.

(33) Marrink, S. J.; Tieleman, D. P. Perspective on the Martini Model. *Chem. Soc. Rev.* **2013**, *42*, 6801–6822.

(34) Moura, A. F. d.; Bernardino, K.; Dalmaschio, C. J.; Leite, E. R.; Kotov, N. A. Thermodynamic Insights into the Self-Assembly of Capped Nanoparticles using Molecular Dynamic Simulations. *Phys. Chem. Chem. Phys.* **2015**, *17*, 3820–3831.

(35) Graupe, M.; Takenaga, M.; Koini, T.; Colorado, R.; Lee, T. R. Oriented Surface Dipoles Strongly Influence Interfacial Wettabilities. *J. Am. Chem. Soc.* **1999**, *121*, 3222–3223.

(36) Sellers, H.; Ulman, A.; Shnidman, Y.; Eilers, J. E. Structure and Binding of Alkanethiolates on Gold and Silver Surfaces: Implications for Self-Assembled Monolayers. *J. Am. Chem. Soc.* **1993**, *115*, 9389–9401.

(37) Dalvi, V. H.; Rossky, P. J. Molecular Origins of Fluorocarbon Hydrophobicity. *Proc. Natl. Acad. Sci. U. S. A.* **2010**, *107*, 13603–13607.

(38) Sergi, D.; Scocchi, G.; Ortona, A. Molecular Dynamics Simulations of the Contact Angle between Water Droplets and Graphite Surfaces. *Fluid Phase Equilib.* **2012**, *332*, 173–177.

(39) Infante, D.; Koch, K. W.; Mazumder, P.; Tian, L.; Carrilero, A.; Tulli, D.; Baker, D.;

Pruneri, V. Durable, Superhydrophobic, Antireflection, and Low Haze Glass Surfaces using Scalable Metal Dewetting Nanostructuring. *Nano Res.* **2013**, *6*, 429–440.

(40) Eghiaian, F.; Schaap, I. A.; Georges, A. D.; Skehel, J. J.; Veigel, C. The Influenza Virus Mechanical Properties are Dominated by its Lipid Envelope. *Biophys. J.* **2009**, *96*, 15a.

(41) Li, S.; Eghiaian, F.; Sieben, C.; Herrmann, A.; Schaap, I. A. T. Bending and Puncturing the Influenza Lipid Envelope. *Biophys. J.* **2011**, *100*, 637–645.

(42) Lakadamyali, M.; Rust, M. J.; Babcock, H. P.; Zhuang, X. Visualizing Infection of Individual Influenza Viruses. *Proc. Natl. Acad. Sci. U. S. A.* **2003**, *100*, 9280–9285.

(43) Rust, M. J.; Lakadamyali, M.; Brandenburg, B.; Zhuang, X. Single-Virus Tracking in Live Cells. *Cold Spring Harb Protoc.* **2011**, *2011*.

(44) Page, K.; Wilson, M.; Parkin, I. P. Antimicrobial Surfaces and their Potential in Reducing the Role of the Inanimate Environment in the Incidence of Hospital-Acquired Infections. *J. Mater. Chem.* **2009**, *19*, 3819–3831.

(45) Greatorex, J. S.; Digard, P.; Curran, M. D.; Moynihan, R.; Wensley, H.; Wreghitt, T.; Varsani, H.; Garcia, F.; Enstone, J.; Nguyen-Van-Tam, J. S. Survival of Influenza A(H1N1) on Materials Found in Households: Implications for Infection Control. *PLoS ONE* **2011**, *6*, e27932.

(46) Dublineau, A.; Batéjat, C.; Pinon, A.; Burguière, A. M.; Leclercq, I.; Manuguerra, J.-C. Persistence of the 2009 Pandemic Influenza A (H1N1) Virus in Water and on Non-Porous Surface. *PLoS ONE* **2011**, *6*, e28043.

(47) Zan, G. H.; Tan, C.; Deserno, M.; Lanni, F.; Lösche, M. Hemifusion of Giant Unilamellar Vesicles with Planar Hydrophobic Surfaces: a Fluorescence Microscopy Study. *Soft matter* **2012**, *8*, 10877–10886.

(48) Meng, H.; Kumar, K. Antimicrobial Activity and Protease Stability of Peptides Containing Fluorinated Amino Acids. *J. Am. Chem. Soc.* **2007**, *129*, 15615–15622.

(49) Vogler, E. A. Structure and Reactivity of Water at Biomaterial Surfaces. *Adv. Colloid Interface Sci.* **1998**, *74*, 69–117.

Graphical TOC Entry

Virus on functionalized surface   Molecular Dynamics simulation of Virus disruption modes   Infectivity